Dependence of exchange bias energy on spin projections at $(La,Ca)MnO_3$ ferromagnetic/antiferromagnetic interfaces

C. Christides[a)]
Department of Engineering Sciences, University of Patras, 26500 Patras, Greece

N. Moutis
Institute of Materials Science, NCSR "Demokritos," 153 10 Athens, Greece

Ph. Komninou and Th. Kehagias
Department of Physics, Aristotle University of Thessaloniki, 54006 Thessaloniki, Greece

G. Nouet
ESCTM-CRISMAT, UMR 6508 CNRS, ISMRA, 6 Bd. du Marechal Juin, 14050 Caen Cedex, France

(Received 27 December 2001; accepted for publication 15 April 2002)

Strained epitaxial bilayers and multilayers consisting of $La_{1-x}Ca_xMnO_3$ ferromagnetic (FM) layers ($x=0.33$, 0.4) and $La_{0.33}Ca_{0.67}MnO_3$ antiferromagnetic (AF) layers were grown on $(001)LaAlO_3$ to study the evolution of exchange coupling interactions. The epitaxy was revealed by conventional and high resolution electron microscopy. An out-of-plane lattice expansion is observed mainly on the FM layers that induces a spontaneous magnetization component normal to the film plane. Field-cooling experiments with the applied field parallel and perpendicular to the film plane exhibit loop-shifts (exchange biasing) and enhanced coercivities that depend on the spin projections at the AF/FM interfaces. © *2002 American Institute of Physics.* [DOI: 10.1063/1.1484230]

I. INTRODUCTION

In 1956 Meiklejohn and Bean observed[1] that isothermal magnetization $M(H)$ loops of cobalt nanoparticles, with a thin layer of antiferromagnetic (AF) CoO coating, could be displaced on the field axis by more than 1 kOe if the particles were cooled in a magnetic field H. This displacement of the $M(H)$ loop manifests the ferromagnetic (FM)–AF form of exchange coupling, which is known as the exchange bias (EB) phenomenon. The EB phenomenon has recently received renewed attention[2] due to its important technological applications to various devices, such as computer disk read heads[3] and pseudo-spin-valve memory elements,[4] that demand an accurate modeling of the magnetization reversal mechanisms involved during an $M(H)$ loop. However, a full understanding of the EB mechanism, free of *ad hoc* assumptions on the interface roughness, is still missing. Recently, Kiwi *et al.*[5,6] have used an EB model, called the frozen interface model, that applies to a large variety of AF/FM systems where the magnetic anisotropy of the AF layer is relatively large, and thus the energy cost of creating a domain wall in the AF is quite considerable. The calculations show[5] that the actual microscopic moment arrangement across the interface of exchange coupled FM/AF layers is such that far from the interface the moments in the AF layer lie on an axis that is orthogonal to the moment of the soft-FM layer at the time of cooling through the Néel temperature T_N. Close to interface the AF-compensated interface monolayer freezes into a metastable, canted magnetic structure that decays within 1 or 2 monolayers of the interface whereas in the FM layer an incomplete domain wall is formed.[6] Thus it is the frozen interface magnetic moment configuration that provides the symmetry breaking necessary to generate an EB field H_{EB} after field cooling (FC).

Of particular interest are the EB properties in colossal magnetoresistance (CMR) compositionally modulated structures consisting of AF/FM $(La,Ca)MnO_3$ layers[7–10] because the involved manganites belong in the category of strongly correlated systems,[11] where the magnetic, electronic, and crystal structures interact strongly with each other. The existence of EB has been revealed[7] at first in $[La_{0.67}Ca_{0.33}MnO_3(FM)/La_{0.33}Ca_{0.67}MnO_3(AF)]_{15}$ multilayers grown on $(001)LaAlO_3$ by pulsed laser deposition. Systematic studies with magnetic and magnetotransport measurements have shown that exchange biasing appears[7–9] below a blocking temperature T_B of about 70 K, that is less than the T_N of the AF layer, where the hysteresis loop $M(H)$ is displaced along the field axis by an amount H_{EB} whereas an increase of the coercive field H_c is observed as well. The origin of such differences between T_B and T_N is a controversial topic in exchange coupled films based on FM and AF oxides due to magnetic proximity effects in the AF/FM interfaces.[12] Specifically, it was observed that the interfacial exchange interactions in CMR artificial superlattices affects systematically both the FM ordering temperatures[13] and the modulation of spin and orbital structures along the stacking direction.[14,15] However, exchange biasing has been reported only in CMR AF/FM multilayers based on combinations of $(La,Ca)MnO_3$ layers with FM $(La,A)MnO_3$ (A=Ca, Sr) layers.[7–9,16]

Since the properties of exchange coupled AF/FM layers depend, generally,[2] on the constituent materials, their thicknesses, and the FC procedure, we have studied the exchange coupling properties of $(La,Ca)MnO_3$ AF/FM multilayers as

[a)]Electronic mail: christides@ims.demokritos.gr

a function of Ca^{2+} concentration,[9] FM and AF layer thicknesses,[8] and the FC and zero field-cooling (ZFC) procedure to understand this preference. It was shown that at the heart of exchange biasing in $(La,Ca)MnO_3$ AF/FM multilayers is the steep decrease of M_{FC} and of the FC resistivity, observed between 5 and 70 K, which are independent from both the AF and FM layer (t_F) thicknesses[8] and the Ca^{2+} concentration or the Mn^{3+}:Mn^{4+} interface ratio used.[9] In a previous study[16] it has been argued that this behavior might not be intrinsic to the AF/FM coupling but it can be induced from extrinsic effects such as disorder, incorrect stoichiometry, and oxygen deficiency. Our latest study[9] shows that although the H_{EB} and FC-H_c fields are affected from the average Ca^{2+} concentration at the FM/AF interfaces, the magnetothermal and magnetotransport properties are not a simple superposition of the constituent FM (hole-doped) and AF (electron-doped) layers. These results indicate that a combination of extrinsic with intrinsic effects is responsible for the observed exchange-bias in this category of exchange-coupled CMR multilayers.

Previous studies[17,18] have shown that the magnetic properties of single FM $(La,Ca)MnO_3$ films are sensitive to local crystal properties and strain fields induced by the lattice mismatch with the substrates (extrinsic effects). The present study has a double purpose. The first target is to correlate the extrinsic effects that appear in $(La,Ca)MnO_3$ AF/FM bilayers and multilayers with the exchange bias properties, using magnetic and electron microscopy measurements. The other target is to probe the spin projections at the FM/AF interfaces, using longitudinal and perpendicular exchange-bias experiments[19] with the applied field parallel and perpendicular to the sample plane. For this reason we focus on the study of $La_{1-x}Ca_xMnO_3$(FM)/$La_{0.33}Ca_{0.67}MnO_3$(AF) structures with $x=0.33$ or 0.4, where the maximum H_{EB} and H_c^{FC} values were observed in the multilayers.[7–9]

II. EXPERIMENTAL DETAILS

The beam of an LPX105 eximer laser (Lambda Physic), operating with KrF gas ($\lambda=248$ nm), was focused on a rotating target. During deposition the substrate temperature was stabilized at 700 °C and the oxygen pressure in the chamber was 0.3 Torr, resulting in a deposition rate of 0.03 nm per pulse. Two multilayers with $[La_{1-x}Ca_xMnO_3(4\text{ nm})/La_{0.33}Ca_{0.67}MnO_3(4\text{ nm})]_{15}$ ($x=0.33$ or 0.4) compositions and the two bilayers with $La_{0.33}Ca_{0.67}MnO_3(45\text{ nm})/La_{0.67}Ca_{0.33}MnO_3(20\text{ nm})$, $La_{0.33}Ca_{0.67}MnO_3(40\text{ nm})/La_{0.6}Ca_{0.4}MnO_3(45\text{ nm})$ compositions were prepared by pulsed-laser-deposition of bulk stoichiometric targets on (001)$LaAlO_3$ single crystal substrates. The multilayers were grown on a 40 nm thick $La_{0.33}Ca_{0.67}MnO_3$ AF buffer layer and their FM, AF layer thicknesses were chosen to be at about the optimum exchange-biasing effect observed.[7–9] In bilayers the AF and FM layer thicknesses were selected in the positive magnetostriction range[17,18] of strained La–Ca–Mn–O epitaxial films, where the magnetic easy axis is along the direction of tensile strain. For brevity, we named the samples by the Ca concentration ratio x/y used.

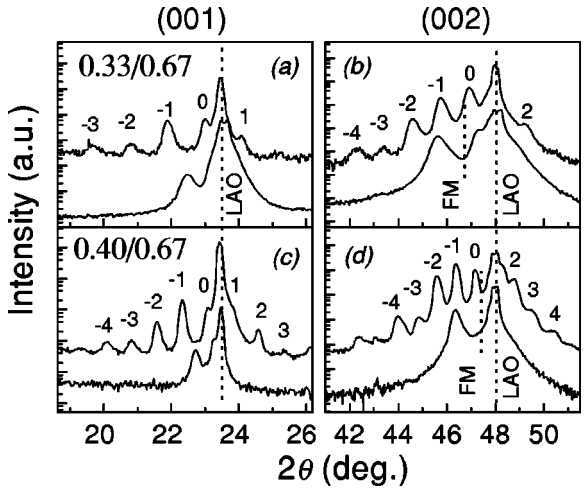

FIG. 1. X-ray diffraction patterns around the (001) and (002) $LaAlO_3$ Bragg peaks (dashed lines). The order of the satellite peaks from the AF/FM superstructure is displayed.

X-ray diffraction (XRD) spectra were collected at ambient conditions with a Siemens D500 diffractometer using Cu K_α radiation. Specimens for cross-section transmission electron microscopy (XTEM) were prepared using the standard techniques of mechanical thinning followed by appropriate ion milling. TEM observations were carried out in a Jeol JEM 120 CX electron microscope operated at 120 kV. In the electron diffraction analysis, the pseudocubic 100 reflection of $LaAlO_3$ was used as a reference for the precise determination of FM and AF $(La,Ca)MnO_3$ interplanar layer spacings, determining a precision of ± 0.002 nm. High resolution electron microscopy (HREM) observations were obtained with a Topcon 002B microscope operated at 200 kV. Magnetic measurements were performed in a Quantum Design MPMSR2 superconducting quantum interference device magnetometer between 5 and 300 K at a maximum applied field of 5.5 T.

III. RESULTS

A. Structural characterization

Figure 1 shows typical XRD spectra of $[La_{0.33}Ca_{0.67}MnO_3(4\text{ nm})/La_{0.6}Ca_{0.4}MnO_3(4\text{ nm})]_{15}$, $[La_{0.33}Ca_{0.67}MnO_3(4\text{ nm})/La_{0.67}Ca_{0.33}MnO_3(4\text{ nm})]_{15}$ multilayers and $La_{0.33}Ca_{0.67}MnO_3(45\text{ nm})/La_{0.6}Ca_{0.33}MnO_3(20\text{ nm})$, $La_{0.33}Ca_{0.67}MnO_3(40\text{ nm})/La_{0.67}Ca_{0.4}MnO_3(45\text{ nm})$ bilayers. The existence of the multilayer structure is confirmed by the presence of multiple satellite peaks (Fig. 1) around the (00ℓ) ($\ell=1$, 2) Bragg-peaks in XRD spectra. Since there are no detectable traces of mixed (001) and (110) textures then gross cumulative roughness effects can be excluded. The grouping of the satellite peaks observed (Fig. 1) nearby the (00ℓ) Bragg-positions of the $LaAlO_3$ substrate indicates that there is a coherent AF/FM superlattice. In multilayers, a multiplet of asymmetric peak intensities appear around the zeroth order (00ℓ) peak due to chemical and/or strained interfacial profiles along the growth direction.[20]

TABLE I. Out-of-plane lattice parameters obtained from XRD and HREM measurements as compared with bulk values of the pseudo cubic unit cell. Note that the parameters are shown separately for FM and AF layers in bilayers whereas in multilayers only an average lattice parameter can be estimated from the XRD data. Each parenthesis includes the estimated error in the last digit.

Sample	XRD-a_p (nm)	HREM-a_p (nm)	bulk-a_p (nm)
0.33/0.67 BL-FM	0.3956(5)	0.399(4)	0.386
0.33/0.67 BL-AF	0.3804(5)	0.386(4)	0.381
0.33/0.67 ML-FM	0.3862(5)	0.390(4)	0.386
0.33/0.67 ML-AF	0.3862(5)	0.382(4)	0.381
0.40/0.67 BL-FM	0.3908(5)		0.3858
0.40/0.67 BL-AF	0.3818(5)		0.381
0.40/0.67 ML	0.3865(5)		

Assuming a pseudocubic structure the observed positions of the fundamental (00ℓ) Bragg peaks allow the determination of the out-of-plane lattice spacings (see Table I). In 0.40/0.67 and 0.33/0.67 bilayers the layer parameters are 0.3908 nm for $x=0.40$ (0.3858 in bulk), 0.3818 nm for $x=0.67$ (0.381 in bulk) and 0.3956 nm for $x=0.33$ (0.386 in bulk), 0.3804 for $x=0.67$, respectively. Evidently, there is an out-of-plane lattice expansion in the FM layers whereas the AF lattice parameters remain close to bulk (relaxed lattice) values in the bilayers due to a small lattice mismatch with the $LaAlO_3$ substrate (0.3792 nm). For this reason we have used an AF buffer layer in the multilayers. Thus an average lattice parameter of about 0.3865 and 0.3862 nm is found in 0.40/0.67 and 0.33/0.67 multilayers respectively, which are close to the lattice parameters of the bulk FM material.

However, in the bilayers there is a significant out-of-plane lattice expansion in the FM layer, which is about 4.3% (2.5%) for $x=0.33$ and 3% (1.3%) for $x=0.4$ relative to a lattice spacing of 0.3792 nm in $LaAlO_3$ (0.386 nm in bulk FM). Notably, the expansion for $x=0.4$ is less than for $x=0.33$, indicating a higher relaxation in the former due to different FM layer thicknesses (45 nm for $x=0.4$ and 20 nm for $x=0.33$) used. It is worth mentioning here that the FM layer thicknesses were selected on the basis of optimal epitaxial registry achieved at the AF/FM interfaces in our samples, to avoid the combination of the inherent complexity of the magnetic structure with many equivalent easy-axes directions that are often present due to atomic arrangement in the vicinity of the interface. Thus the observed out-of-plane lattice expansion can be used in general as an indication for a stress-induced anisotropy in the FM layer, which adds to the total magnetic anisotropy energy. Since the magnetic easy axis is along the direction of tensile strain in strained $(La,Ca)MnO_3$ epitaxial films,[17,18] then the FM layers will have a tendency for an out-of-plane, stress-induced, uniaxial anisotropy.

Previous electron microscopy investigations of the perovskite-manganites have shown[21,22] that the microstructure of these materials includes several typical structural phases and typical types of defect structures including antiphase boundaries and 90° twin related domains. The main results of our study are summarized in Figs. 2–5. A TEM

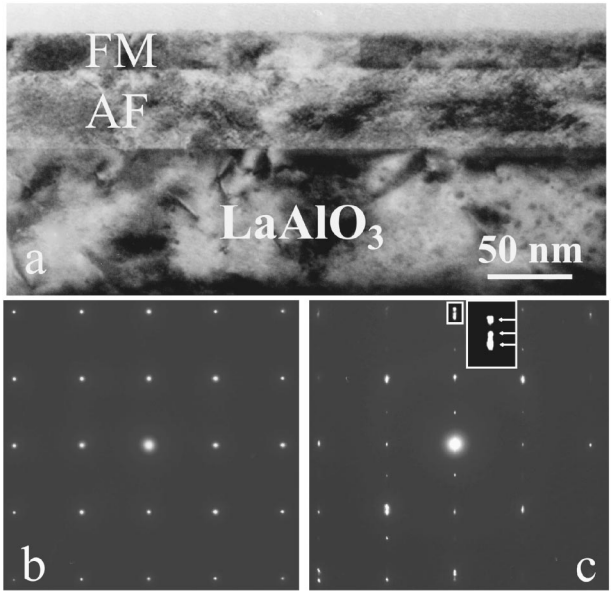

FIG. 2. (a) A bright field cross section TEM micrograph taken along the [001] zone axis from a 0.67/0.33 bilayer, demonstrating the morphology of the system and the sharpness of the $LaAlO_3$/AF and AF/FM interfaces. (b) Electron diffraction pattern from the substrate. (c) Common electron diffraction pattern, taken from the substrate and the bilayer structure.

micrograph in Fig. 2(a) shows a general cross section view of the 0.33/0.67 bilayer whereas in Figs. 2(b) and 2(c) the two electron diffraction patterns (EDP) are given at the same orientation with the image, both taken along the [001] zone axis of the perovskite lattice. Figure 2(b) is the EDP that corresponds to the substrate while Fig. 2(c) shows the common EDP of the bilayer and the substrate. These images indicate a perfect epitaxial registry between the film and the underlying substrate/buffer layer, demonstrating that both epilayers are at the same crystallographic orientation with respect to the substrate. Specifically, the $LaAlO_3$/AF and AF/FM interfaces are parallel to each other without any impurity or amorphous layer. The layer thicknesses in the bilayer are 45 and 20 nm for the AF and FM layer, respectively. A detailed observation of the common diffraction pattern [Fig. 2(c)] shows the following.

(i) If we consider the growth direction to be along [100], by measuring the relative d spacing of the reflections of the three structures that are parallel, and taking the 200 d spacings of $LaAlO_3$ to be 0.3792 nm, the corresponding d spacing of the AF layer is determined to be 0.387 nm and that of the FM layer is 0.398 nm. Thus there is an out-of-plane d spacing expansion along this direction in the epilayers which is clearly illustrated in the magnified image of the second order reflections of the (100) planes [inset of Fig. 2(c)] in the common EPD from the three materials. In this inset the outer diffraction spot corresponds to the substrate, the middle spot to the AF layer, and the inner spot comes from the FM layer. Since the corresponding d spacings in the bulk materials are 0.381 and 0.386 nm, respectively, then the relative expansions are 1.55% and 3% for the AF and FM layers compared to their values in the bulk (Table I). In addition, the observed superlattice reflections in Fig. 2(c) are in agreement with other TEM studies.[21,22]

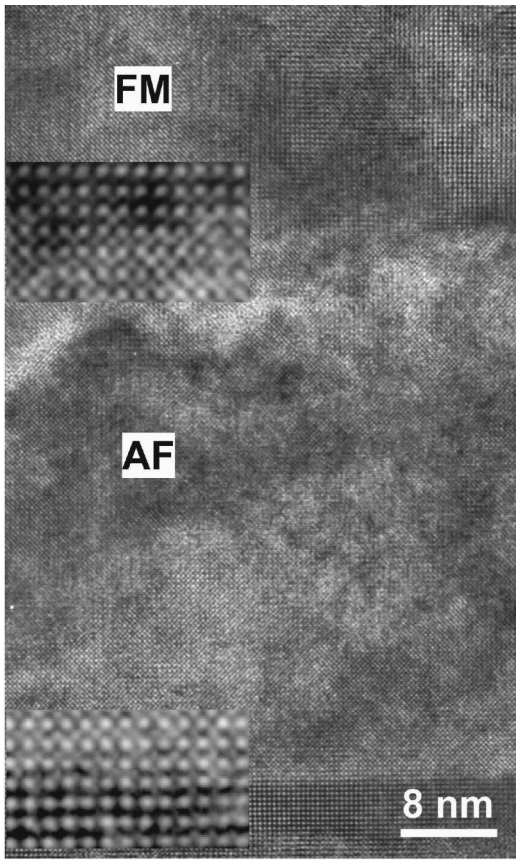

FIG. 3. HREM image viewed along the [001] axis of the 0.67/0.33 bilayer, with insets illustrating the structural arrangement at the interfaces.

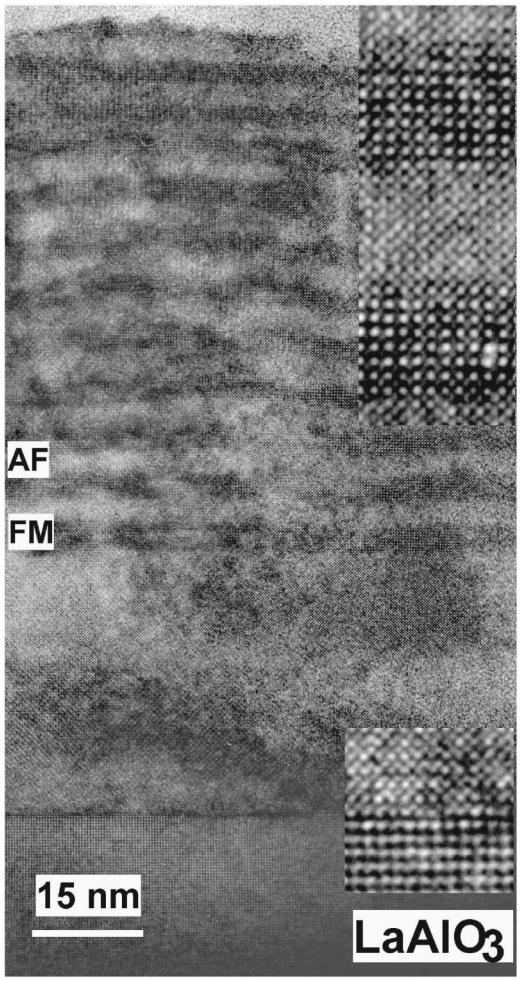

FIG. 4. HREM image of the 0.67/0.33 multilayer with an inset showing a magnified part of the substrate/buffer interface and another inset showing details from the multilayer structure.

(ii) No detectable difference between the (in-plane) d spacing of the $(0h0)$ planes among the three structures is observed. This means that the two epilayers keep almost their bulk in-plane d spacing in the film structure.

The local atomic arrangement of the two heterostructures is illustrated in the HREM image of Fig. 3. Two magnified interfacial parts are given in the insets. As seen, both interfaces exhibit a good epitaxial arrangement. Since lattice fringes from all structures are analyzed in the same image, the d spacings from planes normal and parallel to the growth direction can be measured directly. Thus the relative changes of the d spacing can be calculated with high precision by measuring the length differences from spacings coming from a large number of planes. Using as a reference the spacing of 30 planes from the substrate, the values obtained for the AF and FM layers are 0.386 and 0.399 nm, respectively (Table I), in agreement with the electron diffraction analysis.

Similar measurements have been carried out for the multilayer. Figure 4 shows a typical structure of the multilayer. From this image the thickness of the buffer layer was found to be 35 nm and the thickness of each FM or AF layer is about 3.5 nm. The one inset shows a magnified part of the $LaAlO_3$/AF interface while the other shows an AF layer residing in between two FM layers. The in-plane d spacings in AF and FM layers are similar with their bulk values. The out-of-plane d spacings are 0.382 nm for the AF and 0.390 nm for the FM layers. Thus in both layers the out-of-plane expansion is less than in the bilayer.

Figure 5 shows an HREM image from a FM layer of the bilayer, exhibiting a contrast modulation parallel to $(0h0)$ planes. A periodicity of $2d$ is observed in this image. In agreement with other TEM studies,[21,22] it seems that a general characteristic of the EDP from a FM layer is the existence of extra superlattice reflections. These correspond to multiple periodicities, which appear as a contrast modulation in the HREM images. Such features can be identified[21,22] as domain boundaries that may contribute to the specific magnetic properties of this material.

B. Magnetic measurements

The magnetothermal ZFC and FC curves in Figs. 6–8 were performed by warming up in 100 Oe after having cooled in zero field and 50 kOe (FC) for the $H_{\parallel}$ and $H_{\perp}$ configurations. In 0.33/0.67 samples, Fig. 8 shows only $M(T)$ curves with $H_{\parallel}$ because the $M(T)$ curves with $H_{\perp}$ are almost identical. For direct comparison, the magnetothermal curves of the multilayers with $H_{\parallel}$ are similar with results from Ref. 9. The insets in Figs. 6–8 show in detail the bifurcation of the FC and the ZFC magnetizations. At higher temperatures bifurcation of the FC and ZFC curves occurs between 170 and 255 K (Table II), whereas exchange biasing

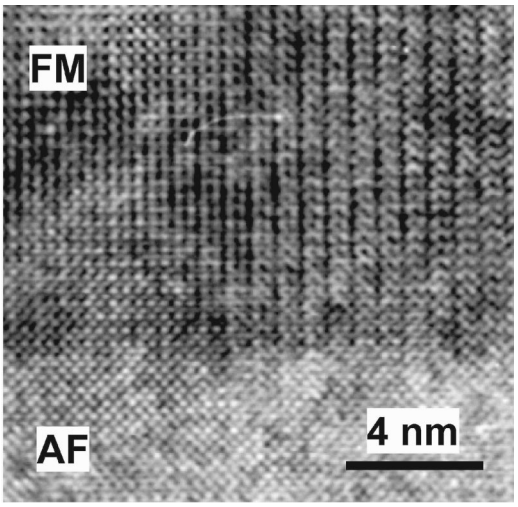

FIG. 5. HREM image taken from a FM area of the 0.67/0.33 bilayer, showing a modulated contrast with a periodicity of $2d$ due to planar defects parallel to the direction of growth.

can be detected only below 70 K. In bilayers the bifurcation of the FC and the ZFC magnetizations appears a few degrees below the Curie point of the FM layers whereas in multilayers the T_{bif} is much lower than the magnetic ordering temperatures of the AF (T_N) and the FM (T_c) layers. This shows that the T_{bif} depends on the number of AF/FM interfaces and the layer thicknesses.

The FC curves exhibit a steep decrease of M_{FC} between 5 and 70 K, that defines[7,8] a T_B in 0.33/0.67 bilayers and multilayers (Fig. 8). In the multilayer the magnitude of M_{FC}

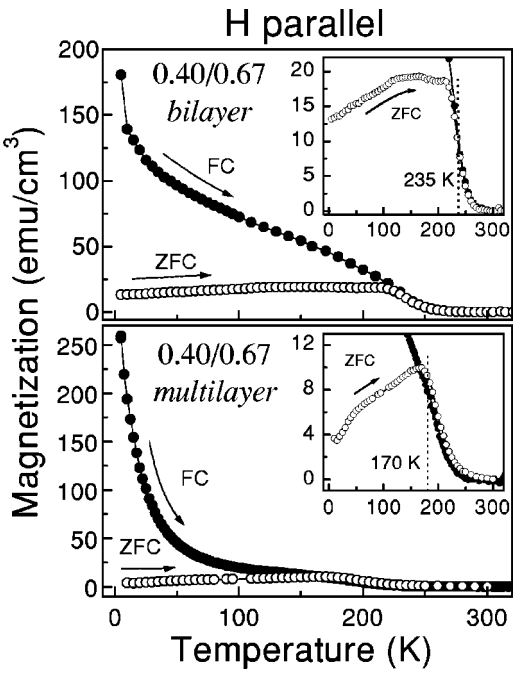

FIG. 6. Magnetothermal measurements from the 0.40/0.67 bilayer and the multilayer, performed by warming up in an applied field of 100 Oe after cooling down from 300 K in zero field (open circles) and 50 kOe (FC, solid circles). For clarity, the insets show the bifurcation between ZFC and FC curves. The magnetization is normalized to the total FM volume of the film used.

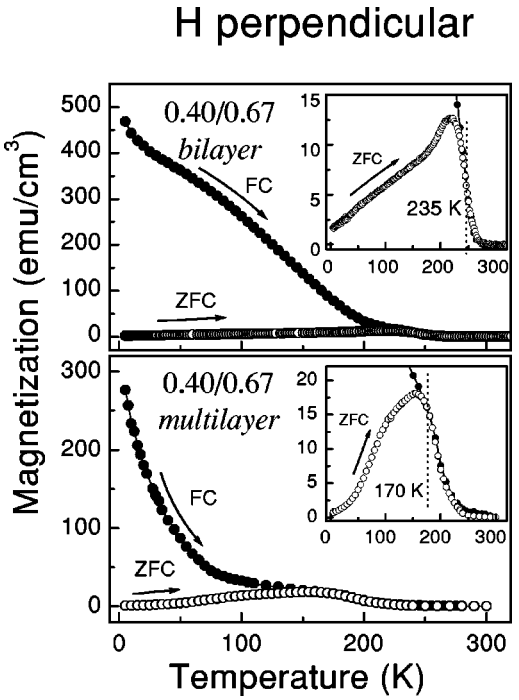

FIG. 7. Magnetothermal measurements from the 0.40/0.67 bilayer and the multilayer, performed by warming up in an applied field of 100 Oe after cooling down from 300 K in zero field (open circles) and 50 kOe (FC, solid circles). For clarity, the insets show the bifurcation between ZFC and FC curves. The magnetization is normalized to the total FM volume of the film used.

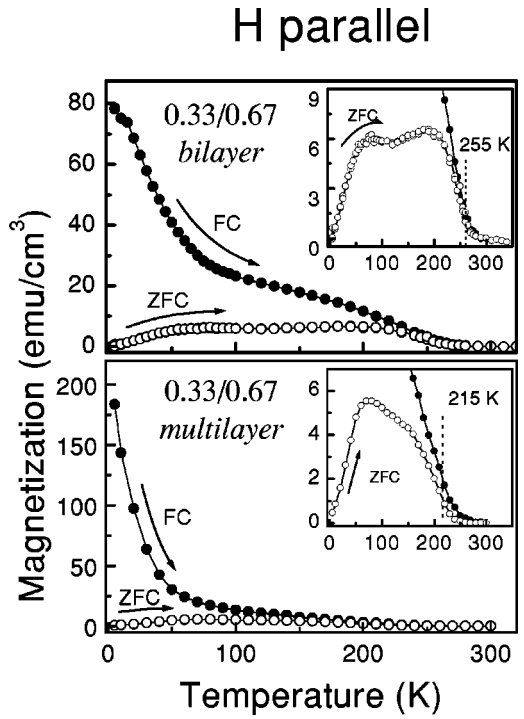

FIG. 8. Magnetothermal measurements from the 0.33/0.67 bilayer and the multilayer, performed by warming up in an applied field of 100 Oe after cooling down from 300 K in zero field (open circles) and 50 kOe (FC, solid circles). For clarity, the insets show the bifurcation between ZFC and FC curves. The magnetization is normalized to the total FM volume of the film used.

TABLE II. Typical H_c^{ZFC}, M_r^{ZFC} values from the ZFC loops and H_{EB}, H_c^{FC}, M_r^{FC} values at 5 K. T_{bif} is the bifurcation temperature. The magnetic fields are in Oe and the magnetizations in emu/cm^3 units.

Sample	$H_{EB}\parallel$	$H_{EB}\perp$	$H_c^{FC}\parallel$	$H_c^{FC}\perp$	$H_c^{ZFC}\parallel$	$H_c^{ZFC}\perp$	$M_r^{FC}\parallel$	$M_r^{FC}\perp$	$M_r^{ZFC}\parallel$	$M_r^{ZFC}\perp$	T_{bif} (K)
0.33/0.67 BL	120	135	710	1830	545	1130	175	360	105	150	255
0.33/0.67 ML	790	340	1245	1510	400	1000	180	160	45	60	215
0.40/0.67 BL	100	150	845	2855	800	2635	155	465	105	420	235
0.40/0.67 ML	640	570	1260	2140	920	2140	220	330	60	170	170

at T_B decreases by an order of magnitude from the M_{FC} at 5 K whereas in the bilayer it becomes about two to three times less and the drop of M_{FC} is less steep. These differences can be associated directly with the larger displacement of the FC-$M(H)$ loops which is observed (Figs. 9 and 10) in multilayers. The spin-glass-like ZFC curves in Fig. 6–8 are independent from the number of AF/FM interfaces and the exchange bias effect. Such ZFC curves resemble the spin-glass-like $M(T)$ curves observed in 100 nm thick $La_{0.67}Ca_{0.33}MnO_3$ films[23] at low T. They arise from microscopic structural distortions due to magnetic microinhomogeneites that are inherent in $(La,Ca)MnO_3$ manganites.[21,23–25] However, it should be emphasized that neither our results nor other studies reveal exchange-biasing effects in single FM or AF thin films.

In 0.40/0.67 bilayers the magnitude of M_{FC} at 5 K with $H_\perp$ is 470 emu/cm^3 (Fig. 7) whereas for $H_\parallel$ it is only 180 emu/cm^3 (Fig. 6). Furthermore, the FC curves with $H_\perp$ do not show a steep decrease of M_{FC} between 5 and 70 K (Figs. 7 and 8). In 0.40/0.67 multilayers the magnitude of M_{FC} at T_B becomes ten times smaller than the M_{FC} value at 5 K for $H_\parallel$ and $H_\perp$, as in 0.33/0.67 multilayers, whereas in the bilayer with $H_\parallel$ it becomes about two times less. The physical origin of these differences can be understood by hysteresis loop measurements.

Typical FC and ZFC loops taken at 5 K are shown in Figs. 9–12. The H_c and H_{EB} fields were derived from isothermal loops at low temperatures after ZFC from 300 K and FC in 50 kOe. The H_{EB} is defined as the loop shift and the H_c as the halfwidth of the loop. Figures 9 and 10 show $M(H)$ loops of the 0.40/0.67 bilayer and multilayer with the external field applied parallel (perpendicular) to the film plane. Figures 11 and 12 show $M(H)$ loops of the 0.33/0.67 bilayer and multilayer with the field applied parallel ($H_\parallel$) and perpendicular ($H_\perp$) to the film plane, respectively. The obtained H_c^{FC}, H_c^{ZFC} coercive fields and remanence magnetization M_r^{FC}, M_r^{ZFC} values are listed in Table II. A measure of the squareness of the loops can be obtained from the ratio of remanent to saturation magnetizations: $SQ=M_r/M_s$, which are listed in the first four columns of Table III. Note that the M_r values from the FC loop were estimated for the symmetric loop shape, which is centered at H_{EB} and not at $H=0$. Apparently, the $M(H)$ loops with $H_\perp$ exhibit more squared loop shapes and larger H_c values than the $M(H)$ loops with $H_\parallel$, that is, more pronounced in the 0.40/0.67 bilayer. These properties indicate that there is a spontaneous magnetization normal to the film.

The FC-$M(H)$ loops with $H_\parallel$ and $H_\perp$ exhibit larger displacement along the field axis in multilayers than the FC-$M(H)$ loops in bilayers (Table II). However, the exchange energy per unit area $J_{ex}=M_sH_{EB}t_F$ should be constant and independent of the t_F since the FM/AF exchange biasing is an interfacial property. Table III displays the estimated J_{ex} values for $H_\parallel$ only because there is a large uncertainty to determine the M_s for $H_\perp$ due to the nontrivial corrections involved (e.g., demagnetization factor, diamagnetic signal from substrate, etc.). Remarkably, the J_{ex} is comparable between the two multilayers and between the two bilayers, within the accuracy of the magnetic parameters involved, but the J_{ex} is different for the two cases. Such deviations in the measurement of J_{ex} between bilayers and multilayers can be explained by the spin projections at AF/FM interfaces. Since magnetic relaxation measurements[10] in these multilayers reveal that the EB energy is

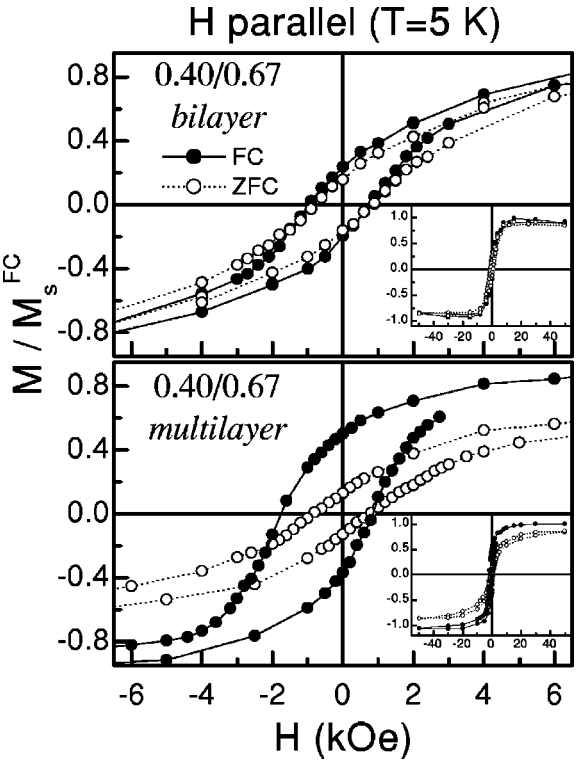

FIG. 9. Magnetic hysteresis loops from the 0.40/0.67 bilayer and the multilayer, measured at 5 K after cooling from 300 K in zero field (open circles) and 50 kOe (solid circles). The external field is parallel with the film plane. The insets show saturation loops in full scale.

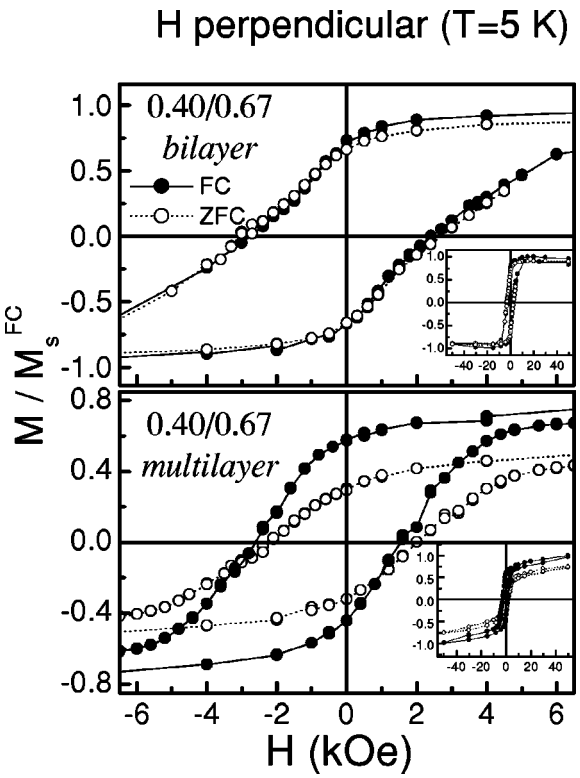

FIG. 10. Magnetic hysteresis loops from the 0.40/0.67 bilayer and the multilayer, measured at 5 K after cooling from 300 K in zero field (open circles) and 50 kOe (solid circles). The external field is perpendicular to the film plane. The insets show saturation loops in full scale.

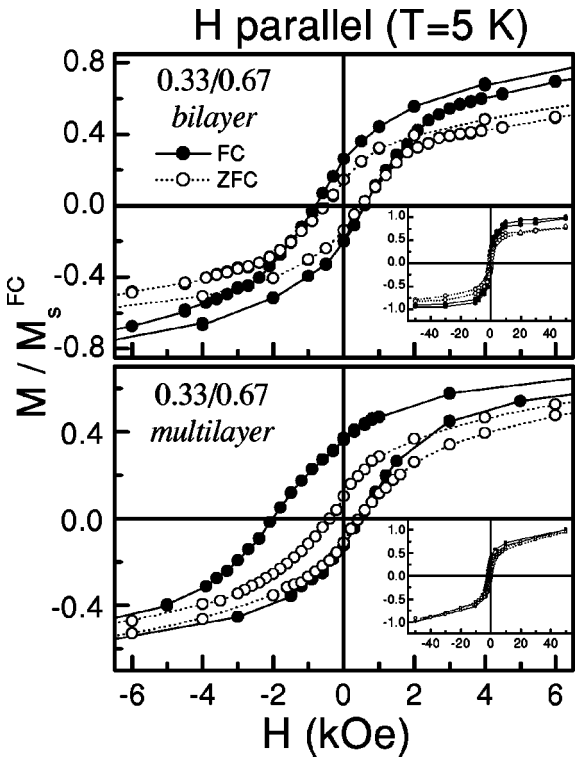

FIG. 11. Magnetic hysteresis loops from the 0.33/0.67 bilayer and the multilayer, measured at 5 K after cooling from 300 K in zero field (open circles) and 50 kOe (solid circles). The external field is parallel with the film plane. The insets show saturation loops in full scale.

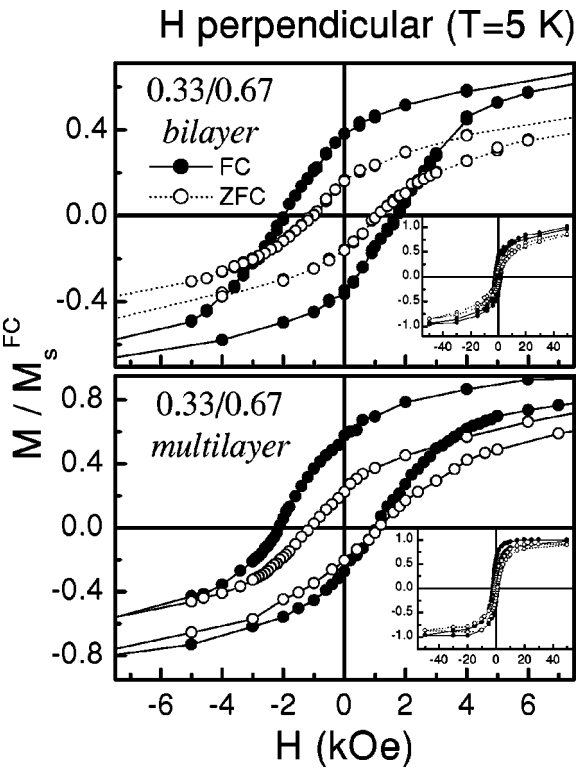

FIG. 12. Magnetic hysteresis loops from the 0.33/0.67 bilayer and the multilayer, measured at 5 K after cooling from 300 K in zero field (open circles) and 50 kOe (solid circles). The external field is perpendicular to the film plane. The insets show saturation loops in full scale.

mainly stored in partial (or incomplete) domain walls in the FM layer, then the frozen interface model of Kiwi *et al.*[5,6] can be used in our case as well. In the Discussion section we explain the role of tensile strain anisotropy on the different J_{ex} values (Table III) obtained between bilayers and multilayers using Kiwi's approximation.[6]

IV. DISCUSSION

In $(La,Ca)MnO_3$ epitaxial films the epitaxial strain is the major source of magnetic anisotropy[17,18] whereas the intrinsic, bulk magnetocrystalline anisotropy is at least an order of magnitude smaller. It was observed[17] that pseudomorphic growth of FM $(La,Ca)MnO_3$ films on $(001)LaAlO_3$ can result in out-of-plane uniaxial tensile strain, inducing an easy axis anisotropy along this direction that may cause a spontaneous magnetization normal to the film. Specifically, the magnitude of an out-of-plane uniaxial anisotropy $K_u \approx 10^6$ erg/cm^3, that is observed[17,18] in strained $(La,Ca)MnO_3$ FM films on $LaAlO_3$, competes with the exchange energy per unit area in exchange coupled AF/FM interfaces,[2,8] $J_{ex} \approx 0.1$ to 1 erg/cm^2, and it can determine the domain pattern in the FM layers. Thus the large out-of-plane lattice expansion observed in the FM layers is expected to determine the direction of the uniaxial anisotropy in the bilayers.

In this study we observe for the first time a strain-induced, out-of-plane lattice expansion in exchange coupled CMR multilayers that stabilizes a spontaneous magnetization component normal to film plane, whereas previous works[17,18]

TABLE III. The loop squareness parameter $SQ=(M_r/M_s)$ is listed at the first four columns. FM layer thicknesses, saturation magnetization M_s^{FC} values extracted from FC loops at 5 K, and the corresponding exchange bias energies per unit area J_{ex} are displayed in the last three columns. The J_{ex} values are estimated from the FC magnetizations with $H_{\|}$ and each parenthesis includes the estimated error in the last digit.

Sample	$SQ_{\|}^{FC}$	$SQ_{\perp}^{FC}$	$SQ_{\|}^{ZFC}$	$SQ_{\perp}^{ZFC}$	t_f (nm)	$M_s^{FC\|}$ (emu/cm^3)	$J_{ex\|}$ (erg/cm^2)
0.33/0.67 BL	0.21	0.38	0.20	0.19	27	690	0.22(2)
0.33/0.67 ML	0.26	0.49	0.11	0.23	4	490	0.15(2)
0.40/0.67 BL	0.24	0.73	0.18	0.73	45	590	0.26(2)
0.40/0.67 ML	0.34	0.50	0.16	0.38	4	480	0.13(2)

report this effect in single FM thin films. The observed epitaxial layer growth does not allow strain-relaxation across the film, resulting in a very strong perpendicular anisotropy that overcomes the magnetostatic energy from the shape anisotropy in multilayers. The obtained $M(H)$ loop shapes (Figs. 9–12) show an inclination of the average magnetization out of the film plane and provide evidence for coexistence of a perpendicular magnetic anisotropy ($K_{\perp}$) with a comparatively large in-plane component of the magnetization due to shape anisotropy. Since at low T the FM and the AF phases undergo a phase transformation from the pseudocubic high temperature structures to low-symmetry phases,[21,23] then below the transition temperature the additional stresses across the interfaces can be an important source for magnetic chirality effects.[26] In principle, such effects can affect mostly the magnetization reversal mechanism in our AF/FM multilayers because the involved manganites belong in the category of strongly correlated systems. This strong interaction can create, among other effects, long range texture that results[27] in phase separation and, of particular interest here, short range texture in $La_{0.67}Ca_{0.33}MnO_3$ thin films. However, despite the strong correlation effects, it was observed[28] that at $\sim$100 K the profile of a magnetic domain wall in 200 nm thick films of $La_{0.67}Ca_{0.33}MnO_3$ can be described in terms of a balance between the quantum mechanical exchange stiffness and any anisotropies present, as in any simple[29] FM material.

Magnetic relaxation measurements have been employed in a recent study,[10] showing that during the magnetization reversal in the FM layer there is no significant reversal in the AF layer which would lead to a variable exchange field acting on the FM domains.[30] In addition, low-field magnetoresistance measurements of tetragonal $La_{0.7}Ca_{0.3}MnO_3$ single FM films[31] suggests that magnetization reversal proceeds by a domain process. Thus based on these experimental results, it is reasonble to assume that on application of a moderate field to exchange-coupled $(La,Ca)MnO_3$ AF/FM multilayers or bilayers, most of the twist in magnetization would occur in the FM layer because the direction of the net sublattice magnetization in the AF layer is fixed by a relatively high uniaxial anisotropy K_{AF}. The additional applied field energy needed to create an interfacial magnetization twist in the FM layer shows up as a shifted $M(H)$ loop that defines the J_{ex} as $M_s H_{EB} t_F$. Thus in order to explain the observed differences of J_{ex} between the multilayers and bilayers we have to consider the effect of strain-induced anisotropy in the stored energy per unit interface area. Among the existing EB models[5] we find it more suitable to use the model of Kiwi *et al.*[6] to do this.

According to this model the compensated AF crystal face at the AF/FM interface freezes in a canted spin configuration below T_N, with a canting angle $\theta_c \neq 90°$ relative to cooling field, whereas an incomplete domain wall is formed in the FM layer. The stored energy per unit interface area depends on[6] the ratios of effective anisotropy $D=K_{FM}/2J_{FM}$ and effective interface coupling $\kappa=-(J_{FM/AF}/J_{FM})\cos\theta_c$ (J and K denote the Heisenberg exchange and anisotropy parameters) and the magnetization vector angle θ_j, of the jth FM monolayer relative to the field cooling direction ($H_{\|}$ and $H_{\perp}$ in this study). Table I shows clearly that the out-of-plane lattice expansion is larger in FM layers than in AF layers, indicating that the projection of spin vector S_{FM} in the adjacent FM interface depends on the stain-induced, out-of-plane anisotropy that adds in K_{FM}. Thus the effect of spin projections, which is a dot product, in interface exchange coupling energy can be described by a Heisenberg spin Hamiltonian:[5] $\hat{\mathbf{H}}_{FM/AF}=-J_{FM/AF}(S_{AF}^{\alpha}+S_{AF}^{\beta})\cdot S_{FM}$, where S_{AF}^{α} and S_{AF}^{β} are canted spin vectors in the AF interface, belonging to the α- and β-AF sublattices, and $J_{FM/AF}$ denotes the Heisenberg exchange parameter which should not be confused with the phenomenological interfacial exchange energy J_{ex}.

Since the discovery of the EB phenomenon,[1] the challenge is to explain why the observed exchange fields are typically of order 1% of this Heisenberg exchange field,[5,32,33] or equivalently, why $J_{ex}(\text{energy/area}) \ll J_{FM/AF} S_{AF}\cdot S_{FM}/a^2$, with a being the lattice spacing. Kiwi *et al.*[6] have shown that the twist of the magnetic spring, or incomplete domain wall, in the FM layer is always less than 20° and thus the small amount of energy stored in the wall is a relevant feature to understand the magnitude of H_{EB}, as well as its overestimate by the early theories.[32,33] In the microscopic model this effect is residing on the dot product, or spin projection term. Our experimental findings in Tables I and III suggest that the addition of an out-of-plane uniaxial anisotropy term K_u ($\approx 10^6$ erg/cm^3), due to uniaxial tensile strain, in the stored energy per unit interface area results in larger J_{ex} for larger out-of-plane lattice expansion in the FM layers. According to Tables I and III this means that a larger elastic energy is stored in the thicker FM layers of a bilayer, causing a more randomized magnetic moment configuration in the AF inter-

face. Thus it is the enhancement of the short range texture that stores additional EB energy in the AF/FM interface of the bilayers relative to multilayers.

V. CONCLUSIONS

In this study we have observed the existence of perpendicular exchange-biasing in CMR multilayers with an out-of-plane easy axis. The interfacial exchange energies per unit area J_{ex} were determined to be about twice as big for the in-plane FC geometry in exchange-coupled AF/FM bilayers than in $(La,Ca)MnO_3$ multilayers (Table III). This difference between the bilayers and the multilayers can be explained by the observed out-of-plane lattice expansion of the FM layers that was observed by XRD, XTEM, and HREM measurements. In addition, the observed $M(H)$ loop shapes show an inclination of the average magnetization out of the film plane and provide clear experimental evidence for coexistence of a perpendicular magnetic anisotropy with a comparatively large in-plane component of the magnetization due to shape anisotropy. As a consequence, the obtained differences in J_{ex} between bilayers and multilayers can be attributed to different spin projections at FM/AF interfaces. Furthermore, it can be argued that spin-freezing of the perpendicular and longitudinal components is the main reason for the steep decrease of M_{FC} and of the FC resistivity, observed in Figs. 6–8 between 5 and 70 K and the FC resistivity reported in Refs. 7–9 as well. Accordingly, the different H_{EB} and H_c^{FC} values in Table II, and those observed in our previous studies[7–9] as a function of the layer thickness or the interfacial Ca^{2+} concentration, can be explained from the different spin projections at FM/AF interfaces that depend strongly on the domain structure in the FM layers. Overall, this work reveals the connection of an extrinsic effect, such as out-of-plane lattice expansion in the FM layer, with systematic changes observed in EB (intrinsic) properties of AF/FM $(La,Ca)MnO_3$ thin films.

[1] W. H. Meiklejohn and C. P. Bean, Phys. Rev. **102**, 1413 (1956); IEEE Trans. Magn. **37**, 3866 (2001).
[2] J. Nogues and I. K. Schuller, J. Magn. Magn. Mater. **192**, 203 (1999).
[3] C. H. Tsang, R. E. Fontana, Jr., T. Lin, D. E. Heim, B. A. Gurney, and M. L. Williams, IBM J. Res. Dev. **42**, 103 (1998).
[4] J.-G. Zhu, Y. Zheng, and G. A. Printz, J. Appl. Phys. **87**, 6668 (2000).
[5] M. Kiwi, J. Magn. Magn. Mater. **234**, 584 (2001), and references therein.
[6] M. Kiwi, J. M.-Lopez, R. D. Portugal, and R. Ramirez, Appl. Phys. Lett. **75**, 3995 (1999).
[7] I. Panagiotopoulos, C. Christides, M. Pissas, and D. Niarchos, Phys. Rev. B **60**, 485 (1999).
[8] I. Panagiotopoulos, C. Christides, D. Niarchos, and M. Pissas, J. Appl. Phys. **87**, 3926 (2000).
[9] N. Moutis, C. Christides, I. Panagiotopoulos, and D. Niarchos, Phys. Rev. B **64**, 094429 (2001).
[10] I. Panagiotopoulos, N. Moutis, and C. Christides, Phys. Rev. B **65**, 132407 (2002).
[11] E. Dagotto, T. Hotta, and A. Moreo, Phys. Rep. **344**, 1 (2001).
[12] P. J. van der Zaag, Y. Ijiri, J. A. Borchers, L. F. Feiner, R. M. Wolf, J. M. Gaines, R. W. Erwin, and M. A. Verheijen, Phys. Rev. Lett. **84**, 6102 (2000).
[13] H. Tanaka and T. Kawai, J. Appl. Phys. **88**, 1559 (2000).
[14] M. Izumi, T. Manako, Y. Konishi, M. Kawasaki, and Y. Tokura, Phys. Rev. B **61**, 12187 (2000).
[15] M. Izumi, Y. Murakami, Y. Konishi, T. Manako, M. Kawasaki, and Y. Tokura, Phys. Rev. B **60**, 1211 (1999).
[16] K. R. Nikolaev, I. N. Krivorotov, W. K. Cooley, A. Bhattacharya, E. D. Dahlberg, and A. M. Goldman, Appl. Phys. Lett. **76**, 478 (2000).
[17] T. K. Nath, R. A. Rao, D. Lavric, C. B. Eom, L. Wu, and F. Tsui, Appl. Phys. Lett. **74**, 1615 (1999).
[18] T. O'Donnell, M. S. Rzchowski, J. N. Eckstein, and I. Bozovic, Appl. Phys. Lett. **72**, 1775 (1998).
[19] S. Maat, K. Takano, S. S. P. Parkin, and E. E. Fullerton, Phys. Rev. Lett. **87**, 087202 (2001).
[20] J. Mattson, R. Bhadra, J. B. Ketterson, M. Brodsky, and M. Grimsditch, J. Appl. Phys. **67**, 2873 (1990).
[21] J. Q. Li, J. Appl. Phys. **90**, 637 (2001).
[22] R. Wang, J. Gui, Y. Zhu, and A. R. Moodenbaugh, Phys. Rev. B **63**, 144106 (2001).
[23] V. K. Vlasko-Vlasov, Y. K. Lin, D. J. Miller, U. Welp, G. W. Grabtree, and V. I. Nikitenko, Phys. Rev. Lett. **84**, 2239 (2000).
[24] J. M. Zuo and J. Tao, Phys. Rev. B **63**, 060407 (2001).
[25] D. Cao, F. Bridges, D. C. Worledge, C. H. Booth, and T. Gebale, Phys. Rev. B **61**, 11373 (2000).
[26] A. N. Bogdanov and U. K. Rößler, Phys. Rev. Lett. **87**, 037203 (2001).
[27] A. Biswas, M. Rajewari, R. C. Srivastava, Y. H. Li, T. Venkatesan, R. L. Greene, and A. J. Millis, Phys. Rev. B **61**, 9665 (2000).
[28] S. J. Lloyd, N. D. Mathur, J. C. Loudon, and P. A. Midgley, Phys. Rev. B **64**, 172407 (2001).
[29] A. Hubert and R. Schafer, *Magnetic Domains* (Springer-Verlag, Berlin, 2000), Chap. 3.
[30] A. M. Goodman, H. Laidler, K. O'Grady, N. W. Owen, and A. K. P.-Long, J. Appl. Phys. **87**, 6409 (2000).
[31] T. O'Donnell, M. Onellion, M. S. Rzchowski, J. N. Eckstein, and I. Bozovic, Phys. Rev. B **55**, 5873 (1997).
[32] C. Mauri, H. C. Siegmann, P. S. Bagus, and E. Kay, J. Appl. Phys. **62**, 3047 (1987).
[33] A. P. Malozemoff, Phys. Rev. B **35**, 3679 (1987); **37**, 7673 (1988); J. Appl. Phys. **63**, 3874 (1988).